High Albedo Interlocking Concrete Block Pavement for Urban Heat Island Mitigation

Original
High Albedo Interlocking Concrete Block Pavement for Urban Heat Island Mitigation / Zhou, Xuan; Ferrari, Chiara; Tefa, Luca; Campagnoli, Elena; Bressan, Maurizio; Mutani, Guglielmina. - In: SUSTAINABILITY. - ISSN 2071-1050. - ELETTRONICO. - 18:4(2026), pp. 1-26. [10.3390/su18041876]

Publisher:
MDPI

Published
DOI:10.3390/su18041876

sustainability

MDPI

Article

High Albedo Interlocking Concrete Block Pavement for Urban Heat Island Mitigation

Xuan Zhou [1], Chiara Ferrari [2], Luca Tefa [3], Elena Campagnoli [1], Maurizio Bressan [1] and Guglielmina Mutani [1,*]

[1] Department of Energy, Politecnico di Torino, 10129 Torino, Italy; xuan.zhou@polito.it (X.Z.); elena.campagnoli@polito.it (E.C.); maurizio.bressan@polito.it (M.B.)
[2] Department of Engineering “Enzo Ferrari”, University of Modena and Reggio Emilia, 41121 Modena, Italy; chiara.ferrari@unimore.it
[3] Department of Environment, Land and Infrastructure Engineering, Politecnico di Torino,10129 Torino, Italy; luca.tefa@polito.it
* Correspondence: guglielmina.mutani@polito.it; Tel.: +39-0110904528

Abstract

The combined effects of global warming and urbanisation have intensified the urban heat island (UHI) phenomenon and thermal stress, especially in the summer season. This study develops an integrated multi-scale framework to quantify the sustainability in terms of the thermal performance of high albedo interlocking concrete block pavement (ICBP) in the city of Turin, Italy. The framework combines: (1) experimental campaigns to establish baseline albedo values, using an albedometer (in accordance with the standard ASTM E1918-21 and E1980-24); (2) in situ measurements to assess the performance of ICBP in three parking areas; (3) satellite analysis using Landsat 8-9 and Sentinel-2 images to derive the land surface temperature (LST) and quantify changes in the surface urban heat island intensity (SUHII). In situ measurements showed an average albedo of 0.20 for ICBP, lower values for aged surfaces and about 0.08 for asphalt. Satellite analysis confirmed the effectiveness of the substitution of asphalt surface pavements with ICBP, revealing an increase of over 30% in both the average albedo and the solar reflectance index (SRI). These results are also combined with the 15% decrease in SUHII. Combining on-site measurements and satellite analysis provides a comprehensive framework for quantifying surface urban heat island effects and thermal performances of more sustainable road pavements. These findings support high albedo ICBP as an effective strategy for UHI mitigation.

Keywords: urban heat island (UHI); surface urban heat island intensity (SUHII); albedo; road pavements; interlocking concrete block pavement (ICBP); remote sensing; climate adaptation

Academic Editors: Guangdong Zhou, Songhan Zhang and Jian Li

Received: 23 December 2025
Revised: 26 January 2026
Accepted: 9 February 2026
Published: 12 February 2026

1. Introduction

Cities are facing increasing challenges from extreme heat events. These are not only driven by global climate change but also by rapid urbanisation. The UHI effect, where urban centre areas show higher surface and air temperatures than nearby rural zones, has become more severe in many cities. This is mainly due to the replacement of natural land cover with man-made materials that have low solar reflectance. These surfaces absorb a large amount of solar radiation during the day and slowly release it at night, raising the urban temperatures and increasing the cooling demand in buildings. Such land cover transformations are observed across diverse geographical and ecological contexts; for instance, research on land-use dynamics in regions such as Meghalaya, India, has

https://doi.org/10.3390/su18041876

highlighted how the transition from natural forest cover to anthropised surfaces alters local environmental stability [1]. At the same time, extreme heatwaves are becoming more frequent, longer, and more intense, especially in densely built areas such as Europe and South Asia [2]. The combined effect of heatwaves and UHI raises thermal risks for urban populations and calls for stronger climate adaptation strategies.

Pavements are one of the main drivers of the UHI effect because they constitute a large portion of urban space, such as roads, sidewalks, parking, and public squares. Their solar reflectance, which is measured by albedo, plays a key role in regulating the surface heat. Common materials such as asphalt and cement concrete tend to have low albedo due to their colour and composition, leading to higher heat storage. In contrast, using high albedo materials is seen as a low-cost and passive strategy to mitigate UHI [3]. In recent years, many studies have explored how increased surface albedo can reduce urban overheating. Some even suggest that albedo interventions could have a small but positive impact on climate, similar to a form of local geoengineering [4], meaning intentional interventions to alter the radiative balance. However, it is crucial to recognise that the mitigation potential of these surfaces is intrinsically linked to the broader urban spatial structure. Studies using fine-scale satellite data, such as those conducted in New York City, NY, USA, by Nath et al. [5], demonstrate that surface temperature patterns are significantly influenced by the heat capacity of materials (which limits the cooling effect of bright surfaces), as well as complex spatial structures, including shadowing effects from variable building heights and trees. This dependency on urban form is further confirmed by Delmastro et al. [6], who highlighted how morphological parameters, such as the height-to-distance ratio and street orientation, critically regulate the urban thermal balance and energy consumption.

As interest in albedo-based solutions grows, there is also greater attention to how albedo is measured. The standard method for field measurement is ASTM E1918, which uses an albedometer to record incoming and reflected radiation on large, uniform surfaces [7]. However, this method has limitations when applied to small, irregular, or obstructed areas. To address these limitations, Qin and He [8] proposed a modified method for small target areas, using shielding and standardised masking to reduce background interference. Other studies, such as that by Sen et al. [9], have also developed theoretical models based on view factors to estimate the albedo of small samples.

The experimental campaign offers further insights into material behaviour under controlled conditions. Chen et al. [10] measured the albedo and internal temperature of asphalt and cement concrete samples with and without surface coatings. Their findings showed that coatings can both increase albedo and reduce the temperature rise, due to their intrinsic reflective properties. García Mainieri et al. [11] demonstrated that asphalt concrete ageing changes surface reflectance, also highlighting the importance of material physical changes.

Beyond campaign work, several field studies have examined the real-world performance of high albedo material surfaces. For example, in 2012, Santamouris et al. [12] carried out the Flisvos project in Athens, systematically evaluating the impact of cool pavements on the microclimate. Their findings indicated that high-reflectance surfaces can significantly reduce both surface and near-surface air temperatures. Similarly, Sen et al. [13], Schneider et al. [14], and Elmagri et al. [15] performed field measurements and large-scale monitoring campaigns in Phoenix, AZ, USA, a representative hot–arid city, to assess and compare the influence of pavements with different albedo levels on the local climate and pedestrian thermal comfort.

Meanwhile, to enable urban-scale analysis, remote sensing has also become a necessary tool. Andrés-Anaya et al. [16] demonstrated, through a study of Spanish cities, that satellite-derived surface albedo and LST exhibit consistent spatial patterns within UHI distributions.

Despini et al. [17] further proposed the use of high-resolution satellite imagery to analyse current land-cover reflectance and to simulate higher reflective coating retrofitting scenarios, quantifying their potential and economic benefits in mitigating UHI.

Despite these efforts, most existing studies focus on only one dimension: either material properties, local thermal response, or urban-scale surface temperature patterns. There is still a lack of integrated studies that link the physical properties of materials with urban content. In particular, the actual climate benefits of reflective pavements under real city conditions remain unclear. Issues also remain about how these pavements perform across different seasons and spaces. Moreover, the long-term performance of materials, which may degrade due to pollution and ageing, has not been fully assessed.

To address these gaps, this study examines three parking areas and a rooftop area in the centre of the city of Turin, Italy. It combines laboratory characterisations, experimental campaigns, in situ field measurements, and satellite analysis. The aim is to assess how more sustainable pavement materials thermally respond under real urban conditions and to evaluate high albedo ICBPs effectiveness in UHI mitigation. The findings are expected to support climate-resilient urban surface design and provide evidence for future policy and planning decisions.

2. Materials and Methods

Given the research objective of evaluating the thermal performance of high albedo materials used in pavement retrofit and their impact on the UHI, the methodological design encompasses Figure 1. Together with albedo and SRI measured by laboratory and campaigns, the LST and SUHII were also calculated using satellite images: these parameters consider solar reflectance and thermal emittance, helping to understand the thermal behaviour of pavements of different materials and characteristics [18].

2.1. Standards and Protocols

Laboratory characterisation of the pavements' materials, allowing for SRI assessment (ASTM E1980-24) [19] by using albedo measurements in accordance with ASTM C1549-16:2022 [20] and ASTM E903-20 [21], was performed. This laboratory measurements campaign, which was essential for the study of materials, allowed for the collection of information about the thermophysical properties under standard conditions, without the influence of the surrounding environment. Reflectance was measured using both a solar spectrum reflectometer (ASTM C1549-16:2022) and a UV-Vis-NIR spectrophotometer (ASTM E903-20), obtaining the value required for the calculation of the SRI and its spectral information. The equipment was conducted using an HD31 multifunction data logger equipped with a matching albedometer, manufactured by Delta OHM company (Caselle di Selvazzano, Padua, Italy). Emissivity is mainly related to the nature of the substrate (i.e., metallic/non-metallic), providing lower or higher values. To measure the thermal emissivity of a non-metallic surface, a 10 cm × 10 cm flat sample is required. Since the ICBP samples present a smaller surface, but the literature provides several thermal emissivity values of these materials, in this work, $\varepsilon = 0.90$ was chosen as a reference value.

Then, albedo measurements according to the ASTM E1918-21 standard [7] were performed, and the SRI was assessed according to the ASTM E1980-24 protocol [19]. The instrumentation consisted of an integrated bidirectional pyranometer (albedometer) that was capable of simultaneously recording incident and reflected solar radiation fluxes. All measurements were conducted under clear, cloudless, and unobstructed weather conditions in July 2025. Measurement sites were selected in open, flat areas that were free of obstructions and surface dust to minimise environmental interference. To comply with the ASTM E1918-21 requirement regarding solar elevation (i.e., the angle between the sun and the normal vector of the test surface must be less than 45°), measurements were conducted between 12:00 and 15:00 local daylight time, ensuring optimal solar altitude and irradiance conditions.

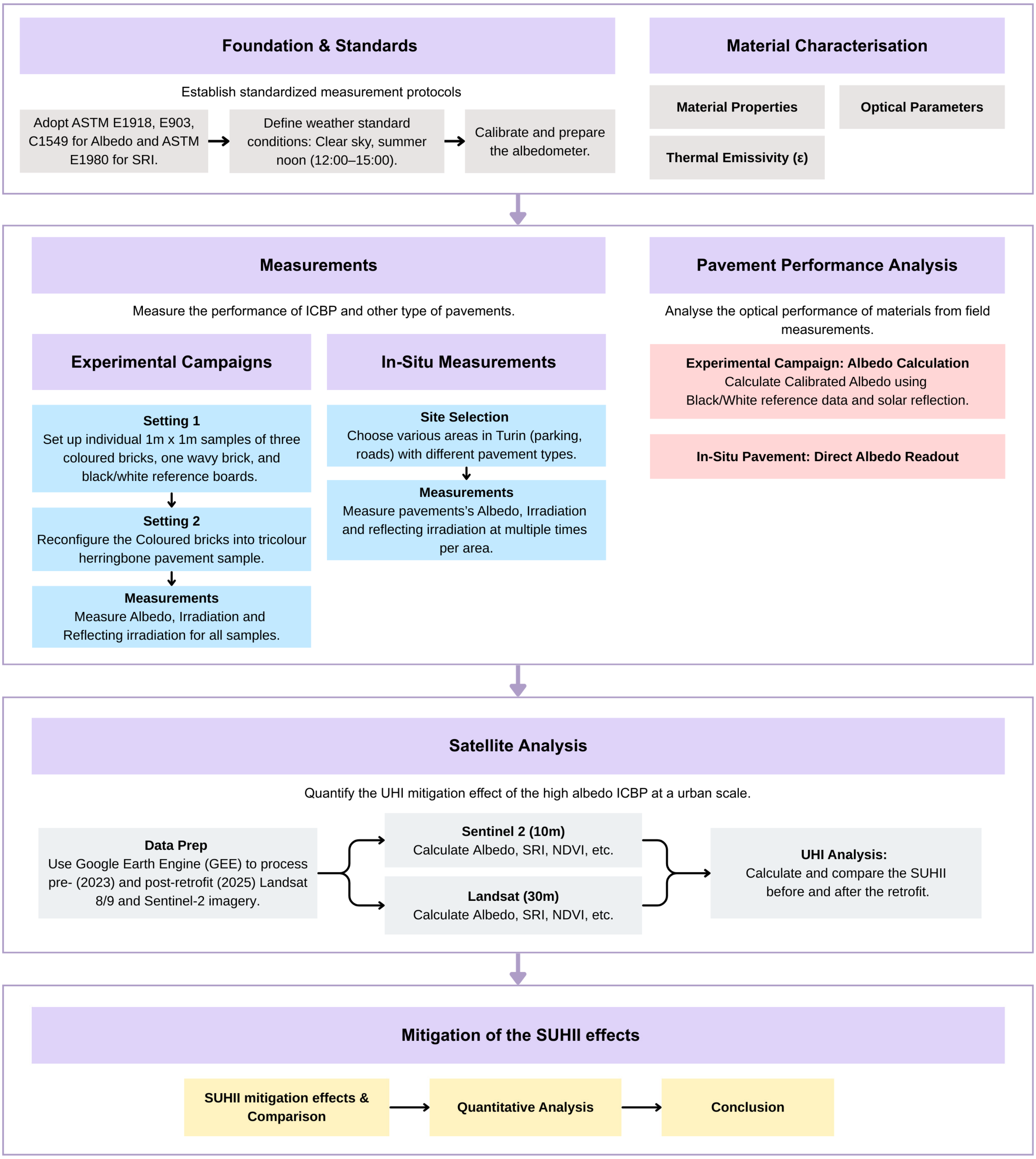

Figure 1. Flowchart of the methodology: data collection, measurements, satellite image analysis and modelling, and evaluation of surface urban heat island effects.

The albedometer was mounted directly above the centre of the test surface at a height of 50 cm. To further ensure the consistency of the albedo measurements and reduce the

https://doi.org/10.3390/su18041876

edge effects, a rod length of 2.45 m was employed in the experimental setup. During each measurement session, the sensor maintained a constant height and orientation while continuously collecting data within the designated area, with the mean value used as the representative albedo reading for the sample. Before installation, the sensor was levelled using a spirit level to ensure accurate, consistent readings of both the incoming and reflected radiation.

2.1.1. Albedo: Laboratory Measurements

The albedo is a parameter that ranges from 0 to 1 and represents the fraction of incident solar radiation reflected from a solar-irradiated surface. It can be measured by using two different methods. The first method, described by ASTM E903, quantify solar reflectance by using a Jasco V-670 UV-Vis-NIR spectrophotometer with an ILN-725 150 mm integrating sphere. In this case, albedo ρ_{sol} is weighted by the standard spectral irradiance of the sun at the Earth's surface as Equation (1):

$$\rho_{sol} = \frac{\int_{300}^{2500} \rho_\lambda \cdot I_\lambda \cdot d_\lambda}{\int_{300}^{2500} I_\lambda \cdot d_\lambda} \tag{1}$$

where ρ_λ is the spectral reflectance at the wavelength λ; I_λ is the standard solar spectral irradiance; d_λ is the wavelength interval and λ represents the wavelength, integrated over the solar spectral range from 300 nm to 2500 nm.

In this study, two different irradiance spectra were used: AM1GH (Clear sky, AM1, global horizontal irradiance), which valorises cool pavement performances, and EN891BN (Hazy sky, AM1.5, beam normal irradiance), which better represents the conditions in Northern Italy [22]. The second method, described by the standard ASTM C1549, uses a multiband solar spectrum reflectometer, SSR V6.0, by Devices and Services, that illuminates the sample by using a tungsten lamp placed inside a cavity coated with high reflecting materials. With this method, albedo is directly measured by weighting data received by six sensors operating at different wavelengths. Both measurements are made in comparison with certified reference samples, which guarantees the traceability of the operations. The uncertainty in the measurements of solar reflectance is ±0.02 [23].

2.1.2. SRI: Laboratory Measurements

The SRI is a parameter that can be obtained by combining albedo, thermal emissivity and the reference wind velocity (to estimate the convection coefficient). It provides information on the equilibrium temperature of an irradiated surface being influenced by how much solar radiation it reflects and how efficiently it emits thermal energy [18].

This parameter can be calculated with reference to a standard white surface (Albedo = 0.8, ε = 0.9, SRI = 100) and a standard black surface (Albedo = 0.05, ε = 0.9, SRI = 0) by using Equation (2):

$$SRI = 100 \cdot \frac{T_b - T_s}{T_b - T_w} \tag{2}$$

where T_b (K) and T_w (K) are the temperatures that would be steadily reached by the two reference samples, while T_s (K) is the temperature of the measured sample.

Under standard solar and ambient parameters, considering the absorptance α (i.e., 1-Albedo), the emissivity ε and the convective coefficient h_c ($Wm^{-2}K^{-1}$), Equation (3) can be used:

$$SRI = 123.97 + 141.35 \cdot \chi + 9655 \cdot \chi^2 \tag{3}$$

where χ is an intermediate parameter, defined as follows:

$$\chi = \frac{(\alpha - 0.029 \cdot \varepsilon)(8.797 + h_c)}{9.5205 \cdot \varepsilon + h_c} \tag{3a}$$

The SRI is calculated using the convection coefficient h_c, which is equal to 5, 12, and 30 $\mathrm{W/m^2/K}$ for low, intermediate, and high wind speeds, respectively. In this study, a h_c value of 12 $\mathrm{Wm^{-2}K^{-1}}$ is used, corresponding to medium wind velocities of 2–6 m/s; this is a standard reference for SRI calculation to ensure comparability, which is consistent with the methodology described by Muscio [18] and the ASTM E1980 standard [11].

2.1.3. Albedometer: Experimental and In Situ Campaigns

The albedometer (model Senseca LP PYRA 06) consists of two coupled spectrally flat class C pyranometers. One measures incident solar radiation, and the other measures radiation reflected from the ground. The radiant energy is absorbed by the black matte-coated surface in the centre of a thermopile, thus creating a temperature difference between the blackened surface and the pyranometer body. The thermopile converts this thermal gradient into a differential electrical voltage, while the radiation energy is derived by knowing the sensitivity of the equipment (in the typical range of 5–15 $\mathrm{\mu V/Wm^{-2}}$).

The measured albedo is defined as the portion of the solar radiation that is reflected from the ground ($E_{reflected}$), with respect to the incident radiation (E_{total}) as Equation (4):

$$\text{Albedo} = \frac{E_{reflected}}{E_{total}}. \tag{4}$$

The thermopiles are enclosed within a 4 mm-thick optical glass dome which protects the sensing surface from environmental effects, while allowing the radiation to pass through with minimal attenuation. The instrument impedance is specified as being between 33 and 45 Ω, and its measurement range extends up to 2000 $\mathrm{W \cdot m^{-2}}$. The manufacturer-declared measurement uncertainty is ±1.8% under the standard calibration conditions, in accordance with ISO 9847 [24].

To improve the accuracy of the measurements, the experimental campaign should be done at noon; when the solar irradiation and the sun height are higher, more radiation is absorbed, resulting in a lower and more stable albedo value.

Moreover, the use of an albedometer requires large samples to ensure that all reflected radiation from the target reaches the downward-facing pyranometer, rather than the surrounding areas [25]. When the sample is smaller, a variation in ASTM E1918 was set up, following E1918a [26]. While ASTM E1918-21 typically requires a target area of at least 10 $\mathrm{m^2}$, this study adopted the 'E1918A' technique described by Akbari et al. [26]. This technique permits the measurement of solar reflectance for smaller surfaces of about 1 $\mathrm{m^2}$. To ensure data accuracy and minimise background interference at this scale, the albedometer was mounted at a height of 50 cm directly above the centre of the module. According to Akbari et al., the difference between E1918A (1 $\mathrm{m^2}$) and the standard E1918 (10 $\mathrm{m^2}$) measurements does not exceed 0.02 to 0.03. This close agreement demonstrates that the 1 $\mathrm{m^2}$ setup is a scientifically sound alternative for comparative material characterisation when space or material availability is constrained.

According to this method, albedo is calculated by using the solar reflectance of white and black masks and the radiation reflected by these masks, and is collected by an albedometer placed as reported in Figure 2 and calculated as in Equation (5):

$$A_s = A_b + \frac{I_3 - I_2}{I_1 - I_2} \cdot (A_w - A_b) \tag{5}$$

https://doi.org/10.3390/su18041876

where the albedo of the sample A_s is calculated by using the albedo and measured by using ASTM E903 of white (A_w) and black (A_b) mask, and the irradiances received by the albedometer are in three different configurations: the target area that is exactly covered by a white solar opaque mask (I_1), the target area that is exactly covered by a black solar opaque mask (I_2) and a target area that is uncovered (I_3).

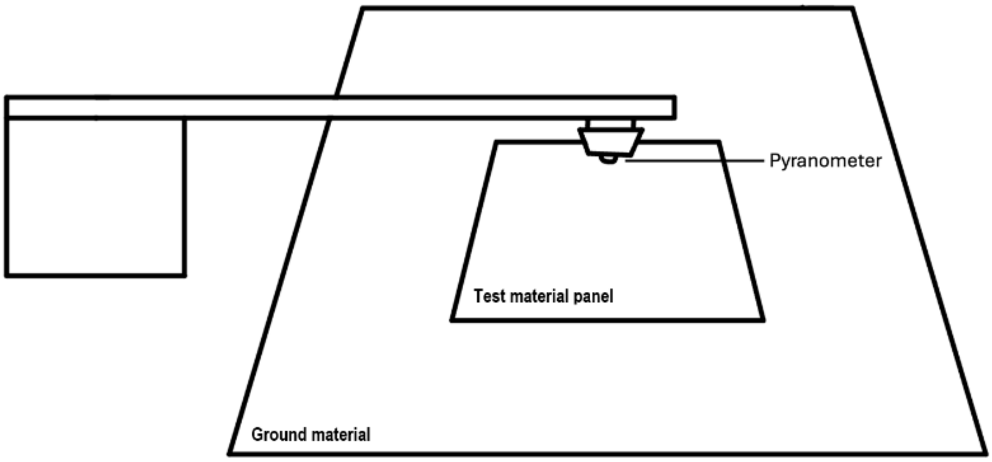

Figure 2. Measurements on the test panel with the E1918a setup.

2.2. Controlled Experimental Campaign

A standardised outdoor test site was established on an unobstructed rooftop platform to assess the solar reflectance and albedo of different paving materials under the same and uniform environmental conditions. Five pavement configurations were prepared: four single-material surfaces, red ICBP, light grey ICBP, dark grey ICBP, and wavy grey ICBP, each arranged in 1.0 m × 1.0 m square modules. A fifth configuration consisted of a tricolour ICBP assembly, combining the red, light grey, and dark grey units to replicate the patterns that are typical of urban pedestrian pavements in Turin.

A minimum spacing of 3 m was maintained between all modules to avoid radiative interference. For each surface, the solar reflectance and SRI were measured using the described albedometer setup and following the procedures outlined in Section 2.1.3.

2.3. In Situ Measurements

To assess the performance of the paving materials under urban conditions, in situ albedo measurements were conducted at selected open-air parking areas and road intersections across the city of Turin. The investigated pavement typologies included a newly installed tricolour ICBP with clean surfaces and saturated colours, along with an older installation of the same pattern exhibiting visible ageing. These two configurations enabled a comparative analysis of optical performance differences between new and aged materials.

Additional pavement types were also surveyed, including yellow ICBP, which is typically installed in drive lanes. Parking bays were generally paved with wavy grey ICBP that provided combined drainage and moderate solar reflectance. Asphalt concrete pavements were included as control surfaces. Both new and worn asphalt were examined due to their ubiquitous presence in urban mobility networks. These reference surfaces were measured in locations such as the plaza and internal roads within the Politecnico di Torino campus.

These pavement types were distributed across multiple survey locations in Turin, including the Via D'Annunzio (Site A), Corso Ferrucci (Site B), and Via Martini Mauri (Site C) parking lots, ensuring both representativeness and broad urban relevance. For reference, traditional asphalt concrete pavement surfaces were also measured; these dark pavements, such as the asphalt in the bike parking of Via Enrico D'Ovidio, represent the most common material in the urban road network.

At each site, measurement points were preferentially located at the centre of the pavement area to minimise the edge effects. The sampling points were located away from pavement edges, vehicle paths, pedestrian flows, and any sources of partial shading. Only dry, unobstructed surfaces were considered. For each pavement typology, data were collected from a minimum of two independent locations to ensure representativeness.

Measurements were carried out between 8–11 July 2025, complying with the requirements of ASTM E1918-21 regarding weather, solar elevation and environmental stability. The resulting data set provides a basis for assessing the real-world solar reflectance performance of common urban pavements and serves as a ground-truth reference for validating remotely sensed albedo estimations in subsequent analyses.

2.4. Satellite Analysis for Albedo, SRI and SUHII

High-resolution optical and thermal variables, especially Land LST and SUHII, are essential for characterising the impact of ICBPs on urban thermal environments. However, Landsat 8/9 provides thermal infrared bands, but at a relatively coarse spatial resolution (30 m), which fails to capture fine-scale urban details such as parking lots. Conversely, Sentinel-2 offers high spatial resolution (10 m) for optical and near-infrared bands but lacks a thermal sensor. To overcome this, this study employs a downscaling framework to synthesise the advantages of both sensors, producing 10 m LST maps that are both spatially detailed and thermally accurate.

Satellite images from Landsat 8-9 and Sentinel-2 were accessed via the Google Earth Engine (GEE) platform. To ensure comparability between pre- and post-substitution of asphalt with ICBPs, two typical cloud-free summer days in each year with nearly similar meteorological conditions (air temperature and solar irradiance) were selected. Because summer is the season when UHI effects are most pronounced and extreme heat events are more frequent, it was suitable for analysing how different pavements respond to high temperature conditions and their potential to moderate heat stress.

Since Landsat 8/9 and Sentinel 2 operate on different acquisition schedules, Sentinel images were selected to match the meteorological context of the Landsat observations. For quality control, only images with less than 10% cloud cover and full spatial coverage were used.

However, in this methodological framework, it is crucial to account for the operational status of the study sites. As highlighted by Matias and Lopes (2025) [27], parked vehicles represent a frequently underestimated contributor to urban warming: metallic vehicles heat rapidly under solar radiation, and their surface temperatures are generally much higher than those of the surrounding concrete or asphalt. Unlike controlled experimental plots, the satellite pixels of the investigated parking lots inherently represent a 'mixed surface' composed of both the pavement material and parked vehicles. Their metallic surfaces and varying colours contribute to the integrated radiative and thermal signals recorded by the sensors. Consequently, the satellite-derived indicators, such as albedo, SRI, and LST, reflect the global thermal performance of the parking area plus vehicles in real usage, but the effect of the different types of pavement can still be noticed (asphalt or ICBP).

In terms of data utilisation, Sentinel-2 was primarily used to extract optical characteristics at 10 m spatial resolution, including albedo and SRI. These indices exhibit relatively low sensitivity to instantaneous meteorological conditions. In contrast, Landsat 8 and 9 imagery was used to derive LST from its thermal infrared band (ST_B10) and to calculate the SUHII. This process is more sensitive to the cloud coverage, solar irradiance, and air temperature.

This study adopts the satellite-based indicators and indexes methodology proposed by Mutani in 2024 [28]. The albedo is calculated using a multi-band weighted average method with Equation (6):

$$Albedo = \frac{\rho NIR + \rho SWIR}{2 \cdot (1 - \rho RED)} \tag{6}$$

where ρNIR is the spectral reflectance in the near-infrared (NIR) band; $\rho SWIR$ is the spectral reflectance in the SWIR band; ρRED is the spectral reflectance in the red band.

The SRI is used to indicate the relative reflectivity of surface features with respect to incoming solar radiation, where SR refers to the solar reflectance of the target pixel. Equation (6) shows the contribution of high-energy spectral regions near-infrared and short-wave infrared (i.e., NIR 0.78–1.4 μm and SWIR 1.4–3.0 μm) to the overall albedo; it incorporates a spectral suppression factor based on the RED band to enhance contrasts among various surface features in visible and near-infrared spectra.

The SRI is used to indicate the relative reflectivity of surface features with respect to incoming solar radiation as Equation (7):

$$SRI = \frac{SR - SR_{min}}{(SR_{max} - SR_{min})} \cdot 100 \tag{7}$$

where SR refers to the solar reflectance of the target pixel, SR_{min} and SR_{max} represent the minimum and maximum reflectance values within the study area, and $NDVI_{min}$ denotes the minimum normalised difference vegetation index (used to measure the quantity and quality of vegetation).

The LST was calculated from the thermal infrared band ST_B10 of the Landsat 8 and 9 Collection 2 Level 2 product. The raw digital numbers were first converted into a top-of-atmosphere brightness temperature, using the official scaling factors. Subsequently, land surface emissivity and atmospheric correction parameters were applied to obtain the temperature raster in degrees Celsius (°C), which can be expressed with Equation (8):

$$LST = \frac{T_B}{1 + \left(\frac{\lambda \cdot \mathrm{T}_B}{\rho}\right) \cdot ln(\varepsilon)} - 273.15 \tag{8}$$

where T_B is the at-satellite brightness temperature (K); λ is the wavelength of emitted radiance (10.895 μm for the effective wavelength of Landsat 8/9 TIR band); ε is the land surface emissivity; and ρ is a physical constant that is equal to 1.438×10^{-2} m·K, which is the Planck's constant composite. The final LST value was converted from Kelvin to Celsius by subtracting 273.15.

To resolve the spatial discrepancy between the 30 m Landsat thermal observations and the 10 m Sentinel-2 multispectral data, this study implemented the area-to-point regression kriging framework (ATPRK) [29]. This method enhances the spatial resolution of LST while strictly maintaining the physical energy balance. The downscaling process, as illustrated in Figure 3, follows a three-stage methodology.

First, a multiple polynomial regression model was constructed to capture the complex, non-linear relationships between LST and the urban surface environment. A total of 100,000 feature pixels were selected. To ensure validation, a five-fold cross-validation strategy was adopted instead of a single random split. This method iteratively used the entire dataset for calibration to avoid sampling bias. The final model accuracy is reported as the average metrics, the coefficient of determination (R^2), root mean square error (RMSE) and mean absolute error (MAE) across the five folds.

A feature set of 15 predictors was built to include surface properties, such as the normalised difference vegetation index (NDVI), normalised difference built up index

(NDBI), normalised difference water index (NDWI), and surface albedo; topographic factors, including elevation, slope, and aspect, which influence solar radiation; and nonlinear relationships were represented using squared and interaction terms, including squared terms of vegetation and built up indices and interaction terms between vegetation, topography, and building density ($NDVI^2$, $NDBI^2$, NDVI × Elevation, NDVI × NDBI, NDVI × Albedo, NDBI × Elevation). In addition, Gaussian-smoothed NDVI and NDBI ($NDVI_{smooth}$, $NDBI_{smooth}$) via a 3 × 3 Kernel are used to account for the spatial heat diffusion of buildings and vegetation.

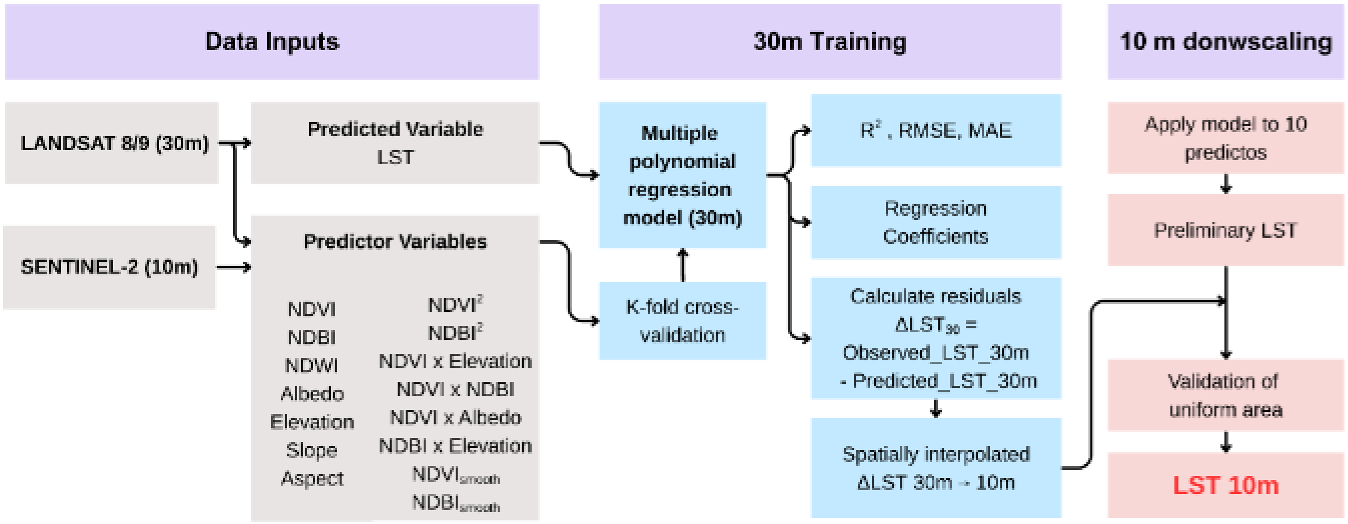

Figure 3. Flowchart about LST downscaling: from 30 m to 10 m.

Second, the model was trained at 30 m resolution to estimate the regression coefficients, which were then applied to the 10 m predictor layers to generate an initial LST trend map. To address the unexplained spatial variability, a residual-correction procedure was applied. Residuals were derived by calculating the difference between the original 30 m Landsat observations and the aggregated mean of the initial 10 m predictions, thereby capturing local thermal differences, such as anthropogenic heat or vegetation/water variations. These 30 m residuals were then spatially interpolated and re-integrated into the 10 m LST map.

Furthermore, to assess physical fidelity, six types of uniform surfaces from the Urban Land Cover with the same pavement material were selected for validation: forest in the hills, water bodies, high-density building district, open square, park grass, and industrial buildings. In these areas, downscaled predictions are expected to closely match observations.

This approach not only increases the urban topology textures, which accurately demonstrate features like buildings and parking areas, but also ensures area-to-point energy consistency to make sure that the values of the 10 m LST remain equal to the original Landsat observations.

To quantify the spatial thermal differences in urban areas, this study employed a statistical approach to calculate the SUHII. Unlike the conventional SUHI definition, which relies on the LST difference between urban and rural reference areas, this study adopts the intensity to avoid the definition of what is urban and rural. This approach normalises the LST of each pixel against the thermal context of the entire study area, thereby enabling comparisons of warmer or colder surfaces in a city.

The LST values in the pavement area corresponding to the pre- and post- retrofit were extracted, and SUHII was calculated to evaluate the changes related to the pavement interventions by following Equation (9):

$$SUHII = \frac{\mathrm{LST} - \mathrm{LST}_{\mathrm{mean}}}{\mathrm{LST}_{\mathrm{stdev}}} \quad (9)$$

where positive SUHII values indicate warmer effects with respect to the average neutral condition $\mathrm{LST}_{\mathrm{mean}}$ with SUHII = 0, and negative SUHII values mean colder areas.

In addition, the remote sensing estimates were integrated with field-based measurements to assess the mitigation effect of higher-albedo ICBP on the UHI phenomenon. Firstly, the albedo and SRI derived from Sentinel-2 were compared with albedometer field measurements to characterise the optical properties of the pavement materials. Then, LST and SUHII were used to evaluate and compare the effects of the surface thermal environment.

3. Case Study: Turin

This study focuses on the city of Turin in the North-West part of Italy. Situated at the intersection of the Po River plain and the Alps, Turin is surrounded by mountains, which limit air movement and contribute to warmer and humid climate conditions during summer. According to historical data from ARPA Piemonte [30], the average maximum temperature during summer in Turin rose from approximately 29.1 °C in 1990 to 31.4 °C in 2023, along with a notable increase in the frequency of extreme hot days. These changes indicate a growing exposure to heat-wave stress, driven by both climate change and the growth of urbanisation.

In response, the Turin municipal government introduced the Torino Climate Resilience Plan in 2022 [31]. Some mitigation measures were adopted, including: reduction in land use, more use of green and vegetation, more permeable surfaces and high-albedo materials. Among these strategies, the substitution of asphalt with ICBPs is considered to be a key intervention. According to international guidelines, the American LEED standard recommends that hardscape surfaces such as roads, sidewalks, and parking areas should have a minimum solar reflectance of 0.33, remaining above 0.28 after 3 years. Similarly, GBC Italia encourages the use of light-coloured paving materials that offer both high reflectance and permeability to reduce the solar radiation absorbed in urban spaces.

The roads play a significant role in shaping urban thermal conditions. In some districts of Turin, asphalt concrete surfaces cover from 36% to 51% of the total ground coverage [32], making them an important contributor to the UHI effects. Conventional asphalt pavements, with their low albedo, absorb a considerable amount of solar radiation during the day and slowly release heat during the night, often resulting in higher urban temperatures than in nearby suburban areas. As such, upgrading pavement systems is considered to be an effective approach in managing the rise in surface and air temperatures.

In this context, Turin, in collaboration with the Italian Ministry for the Environment, proposed a project to mitigate UHI through surface material of roads, sidewalks and parking areas. Then, several typical parking areas were selected for renovation, improving solar reflectance and permeability, thereby reducing the ground temperatures and enhancing the stormwater drainage capacity.

This study focuses on three urban car parking areas in Turin, which were renovated in 2024. The aim was to assess the thermal performance of high-albedo surfaces in real urban environments. As shown in Figure 4, the selected sites are all located in the city centre: (1) Site A, which was renovated from March to June 2024; (2) Site B, for which the main area was renovated from February to June 2024, and the inner area from September to October 2024; and (3) Site C, which was renovated from June to October 2024. Before renovation, all sites were covered with traditional asphalt surfaces. After the intervention, high-albedo ICBPs were installed.

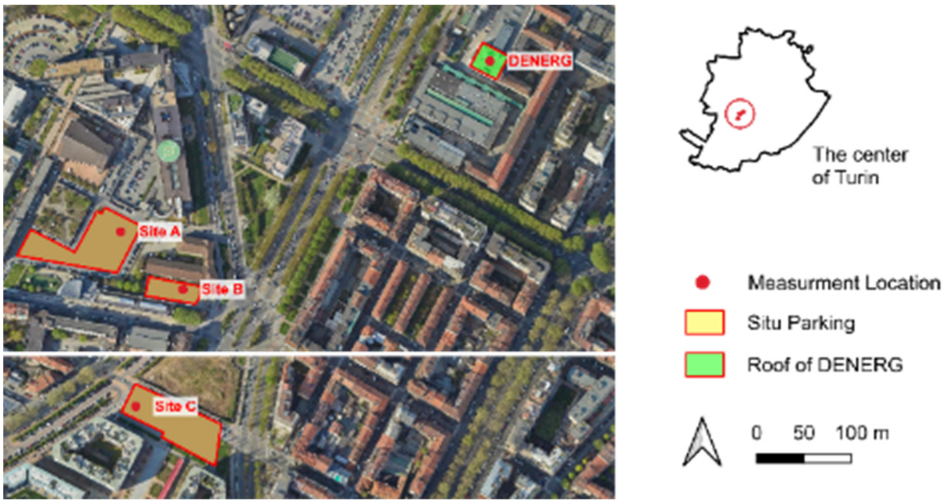

Figure 4. Case-study parking areas for in situ measurements and the experimental campaign site on the flat roof of the Department of Energy (DENERG) of Politecnico di Torino: Via D'Annunzio (Site A), Corso Ferrucci (Site B), and Via Martini Mauri (Site C) parking lots,.

To minimise the influence of environmental variables and enable controlled comparison, a roof site was set up at the Department of Energy, Politecnico di Torino (DENERG). This site was used to evaluate the reflection performance of different pavement materials under the same conditions.

Figure 5 shows the site characteristics of the three car parking areas and the roof of DENERG. All three parking areas are paved open spaces, surrounded by dense built district and complex urban environments. In contrast, the roof site is more unobstructed and consistent in background conditions.

Figure 5. Study area's environment, photographed at noon in July 2025. In situ: (**a**) Site A, (**b**) Site B, and (**c**) Site C. Experimental campaign: (**d**) DENERG rooftop area.

The ICBP used by the city of Turin for the parking areas have a dimension (length, width, and height) of 20 × 10 × 8 cm^3, a weight of ∼3.4 kg, and a density of ∼2102 kg/m^3; only the yellow ICBP has different dimensions (length, width, and height) of 10 × 10 × 8 cm^3. To have more permeable areas, bigger ICBPs with wavy cracks are also used; this ICBP is called "wavy" and it has dimensions (length, width, and height) of 50.5 × 25 × 9 cm^3, a weight of ∼27 kg, and a density of ∼2750 kg/m^3; these cracks amount for the 13% of volume and these will influence the albedo measurements. These ICBPs are made up of aggregates (stone material), cement (the binder) and additives. The aggregates used in northern Italy are typically of alluvial (river) or quarry (carbonate) origin. Alluvial aggregates have a predominantly siliceous composition (quartz/feldspar), while carbonate aggregates are typically rich in limestone ($CaCO_3$) and dolomite ($CaMg(CO_3)_2$).

Depending on the type of cement, the chemical composition can vary. In northern Italy, Portland limestone cements (classified as CEM-II) are used, containing CaO, SiO_2, Al_2O_3, Fe_2O_3, and small amounts of gypsum ($CaSO_4$ $2H_2O$). Finally, the chemical composition also depends on surface treatments and pigments; some useful references are [33,34].

In the experimental campaigns on the roof, various typical urban surface samples were installed, including different colours of ICBP, white and black foam panels, and background surfaces. In situ, samples from the parking pavements were also measured and analysed. In total, 18 representative urban pavement surfaces were examined, as shown in Figure 6.

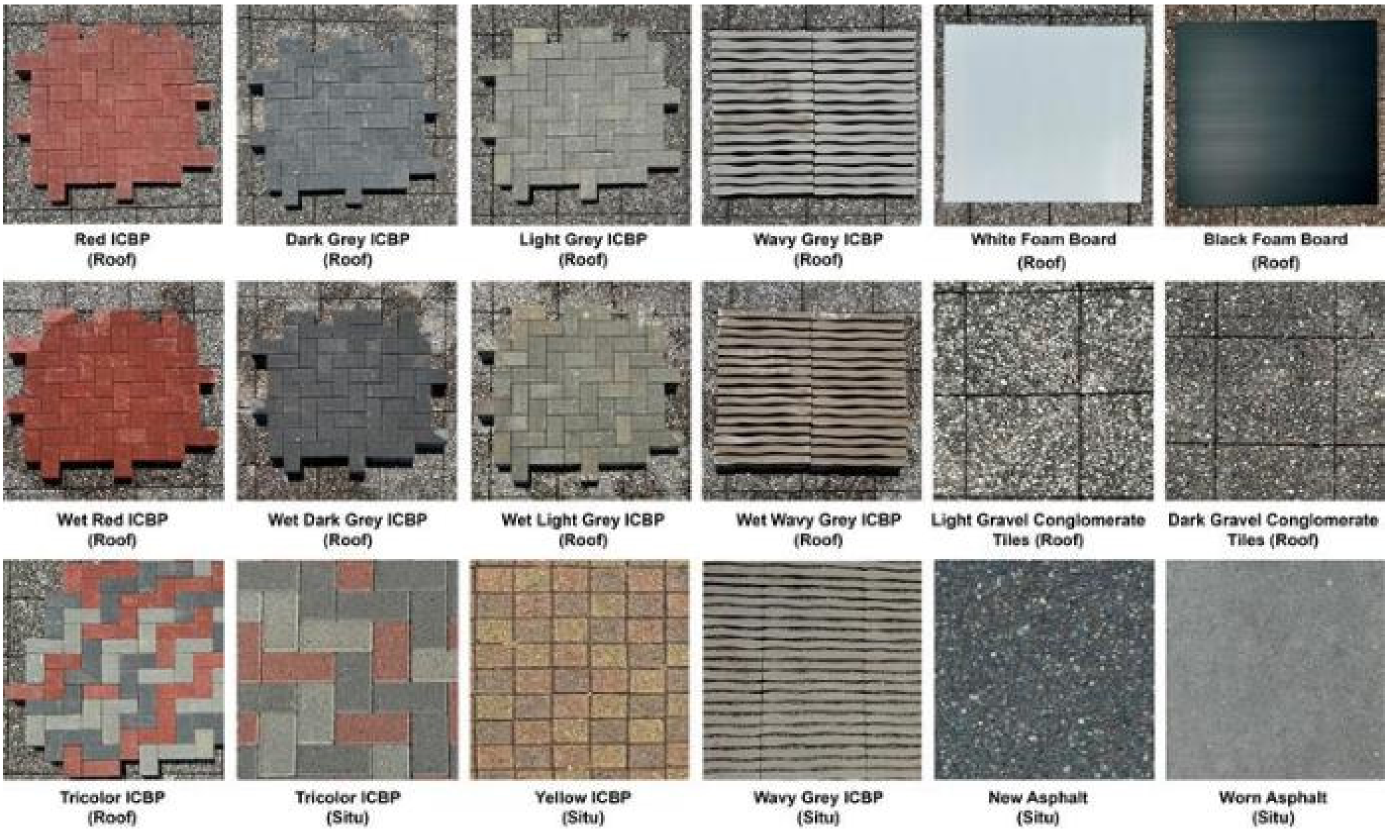

Figure 6. Pavement materials analysed in this study, photographed at noon in July 2025. "Roof": experimental samples of 1 m^2 on DENERG rooftop; "Situ": in situ pavement surfaces.

The results of laboratory and experimental campaigns were then compared with the satellite imagery recorded by Sentinel-2 and Landsat 8 and 9 to evaluate the impact of the pavements for parking areas on the UHI phenomenon. For Turin, satellite imagery is recorded from 10:10 to 10:40 a.m.

Considering the economic point of view, the cost of outdoor pavements varies depending on the material and installation. In Turin, interlocking pavement, including installation, generally costs between €30 and €55/m^2 [35]. Asphalt pavement is less expensive, often between €15 and €30/m^2 depending on the thickness [35], making it the most used solution for parking areas.

Replacing all asphalt roads in Turin with ICBP would be too expensive for the entire city. Although asphalt is cheaper to install, it makes the city hotter and prevents water from passing through. Therefore, a better solution is to only use high-albedo ICBP in specific areas, such as the parking lots in this study. This approach provides major environmental benefits where they are needed most, without the huge cost of changing the entire road network.

4. Results and Discussion

4.1. Material Characterisation

Solar reflectance was measured by using a UV-Vis-NIR Spectrophotometer. Measurements were integrated over the measurement range both by using AM1GH and the EN891BN irradiance spectrum. Both the irradiance spectrum and the spectral reflectivity are reported in Figure 7. From all these samples, it emerges that the spectral reflectivity is evenly distributed across the whole solar spectrum. When analysing the single bands, in the visible range (400–700 nm) the only sample that presents a spectrally selective behaviour, as expected from its visual response, is the red one, with an increase in reflection of around 600 nm. On the NIR range (700–2500 nm), the samples can be divided into three sets: asphalt and dark grey samples present a lower NIR reflectivity, cement deeply decreases the spectral reflectivity after 1800 nm, while wavy grey, light grey and red present a similar behaviour across the NIR Wavelength Range. After the solar reflectance calculation, the results from both the E903 and C1549 measurements can be found in Table 1. Except for the asphalt values, which are lower than 0.2, all the measured reflectance remains between 0.2 and 0.3, indicating homogeneous values that are typical for traditional non-solar reflective paving solutions.

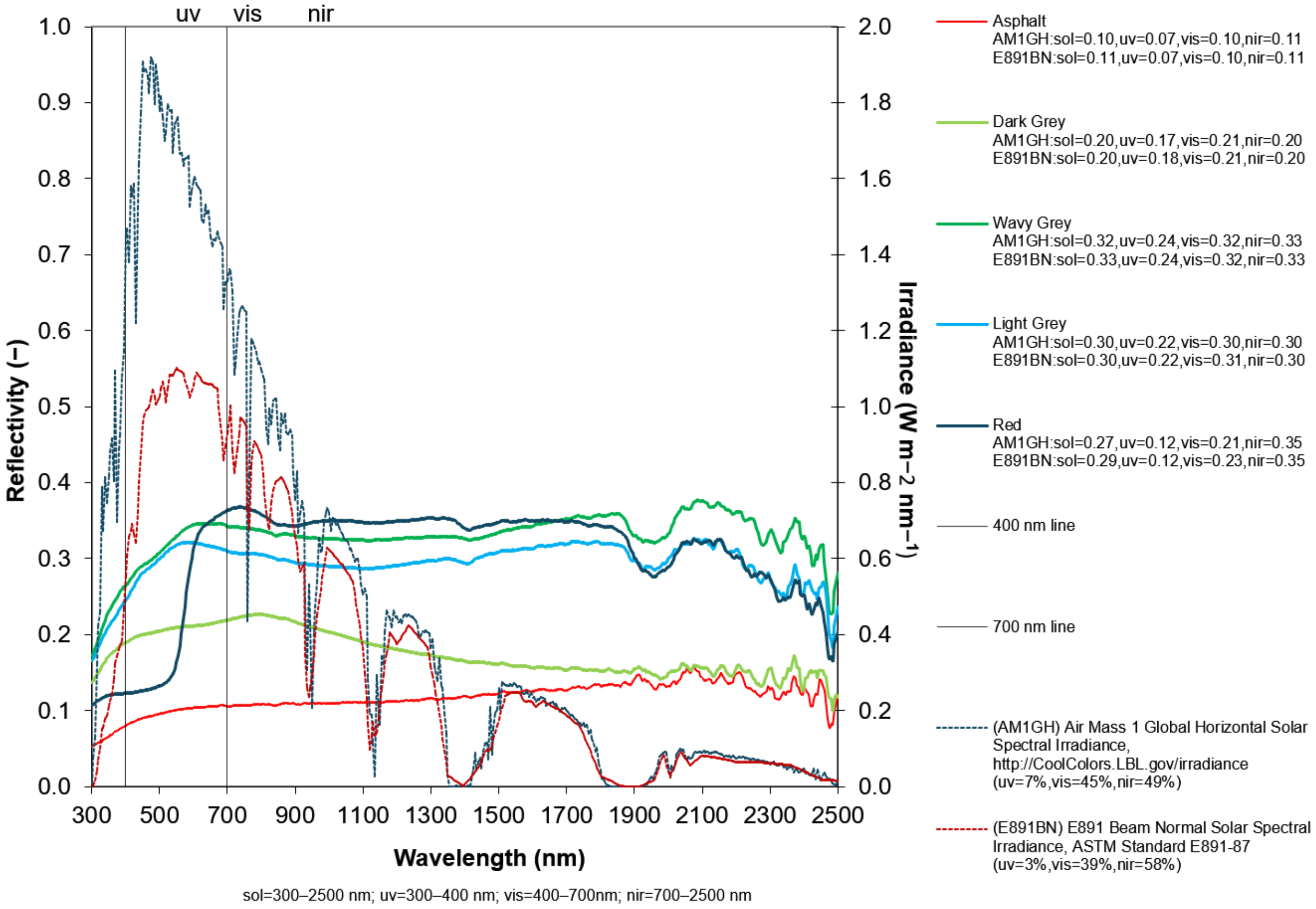

Figure 7. Spectral reflectivity of analysed samples' wavelength from 300 to 2500 nm; the solar reflectivity according to AM1GH and E891BN is reported on the legend by spectral range.

Table 1. Solar reflectance measurements.

Sample		Albedo_C1549	Albedo_E903
White Foam Board	AM1GH	0.734	0.708
	ASTM B891	0.752	0.715
Black Foam Board	AM1GH	0.050	0.047
	ASTM B891	0.047	0.047
Asphalt	AM1GH	0.121	0.107
	ASTM B891	0.123	0.107
Dark Grey ICBP	AM1GH	0.249	0.197
	ASTM B891	0.222	0.197
Wavy Grey ICBP	AM1GH	0.340	0.320
	ASTM B891	0.344	0.330
Light Grey ICBP	AM1GH	0.313	0.293
	ASTM B891	0.314	0.300
Red ICBP	AM1GH	0.277	0.273
	ASTM B891	0.294	0.293

Analysing these data and elaborating on them by using the SRI equation, the data reported in Table 2 can be observed. These data also confirm what is observed in Table 1: the concrete sample presents a very low SRI that, therefore, significantly increases surface temperatures under solar radiation, while all other samples present similar values for SRI.

Table 2. SRI values for analysed pavements.

Sample	SRI
White Foam Board	93
Black Foam Board	0
Asphalt	8
Dark Grey ICBP	21
Wavy Grey ICBP	36
Light Grey ICBP	33
Red ICBP	30

4.2. Pavement Measurements on Experimental Campaign

Experimental campaigns were conducted to evaluate the albedo performance of various pavement materials under controlled conditions, as illustrated in Figure 8. All reflection readings were initially recorded as direct albedo values, using an albedometer.

Figure 9 presents the results of the experimental campaign of the rooftop of DENERG, where the albedo performance of the pavement samples of 1 m^2 was evaluated from 8 to 16 July 2025, in the "noon" hours from 12 a.m. to 3 p.m. The white foam board measured the albedo value of 0.45 to 0.50, while the black foam board ranged from 0.15 to 0.19. Background measurements of the roof pavement showed an albedo of 0.24 for dark concrete and 0.31 for light concrete. Regarding the ICBP samples, the light grey showed an albedo of 0.28–0.29, the dark grey 0.21–0.23, the red 0.25–0.27, and the wavy grey ∼0.27. Additionally, the tricolour ICBP recorded a measured albedo of ∼0.22. To complete this analysis, the albedo of ICBPs was also measured in wet conditions, and its values decreased significantly. Under wet conditions, the albedo of the wavy grey dropped to 0.20, the light grey to 0.19, the red to 0.19, and the dark grey to 0.15.

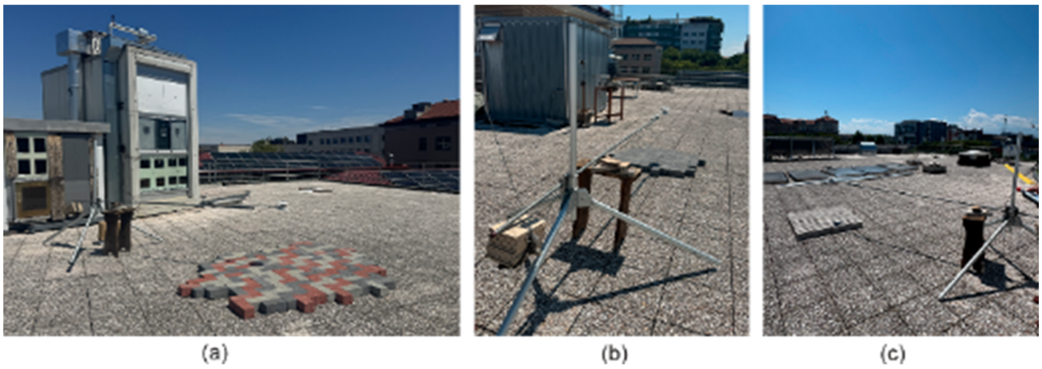

Figure 8. Examples of albedo measurements on the roof: (**a**) tricolour ICBP; (**b**) dark grey ICBP; and (**c**) wavy grey ICBP.

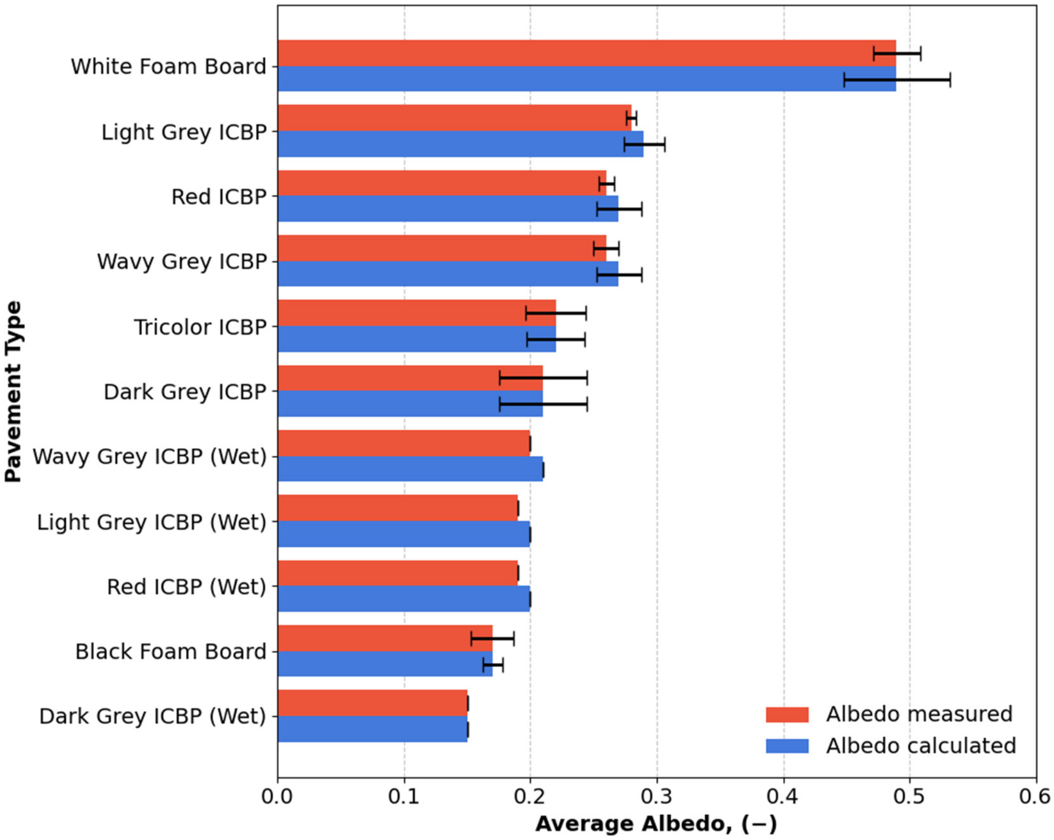

Figure 9. Comparison of average albedo values measured and calculated for different pavement materials: albedo measured vs. albedo calculated with the E1918A technique.

To eliminate sensor and environmental bias, raw data were post-processed using the ASTM E1918A technique. These results highlighted the average albedo values: the light grey ICBP as the highest performer at 0.29, followed by the red and wavy grey ICBPs at 0.27. The tricolour ICBP showed an adjusted albedo of 0.22, which was comparable to the dark grey ICBP, which resulted in a final value of 0.21. Comparison of measured and adjusted data using the E1918A technique confirms the measurements' stability, with minor refinements to account for the border effects during the measurement of the 1 m^2 test panel. This slight upward adjustment is primarily due to correcting for diffuse-sky radiation interference and background, which the direct measurement method slightly underestimates due to the limited panel size.

4.3. Pavement Measurements In Situ

Field measurements were conducted to assess the real albedo values of different pavements at multiple times and sites between 8–16 July 2025, at 12 a.m.–3 p.m., as shown as examples in Figure 10. And the result of average measured albedo of pavements is demonstrated as Figure 11.

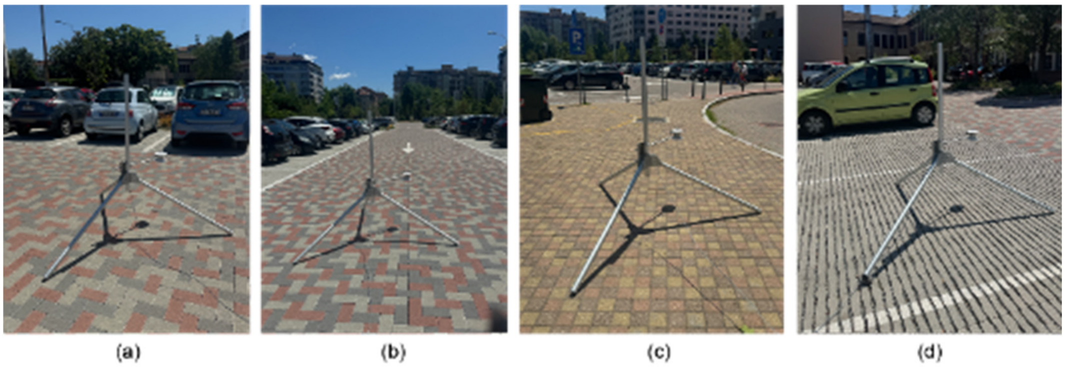

Figure 10. In situ albedo measurements in urban parking: (**a**) Site A; (**b**) Site B; (**c**) Site C; and (**d**) Site B.

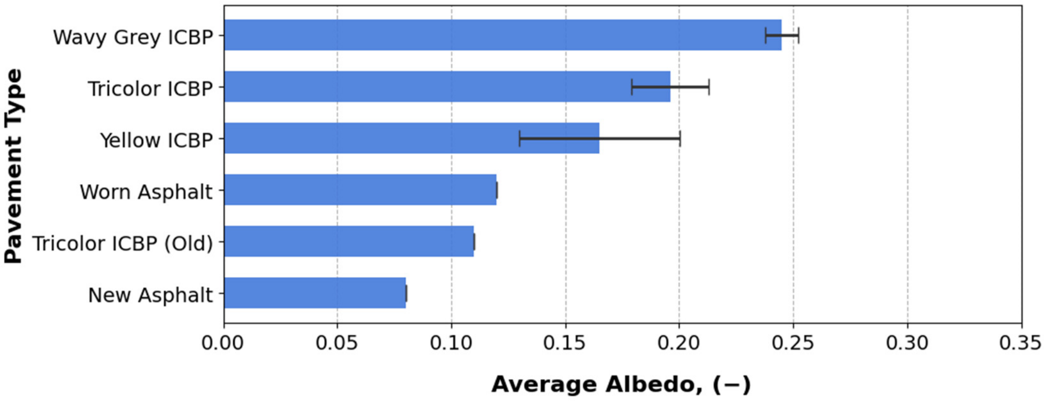

Figure 11. Average albedo (–) values measured in situ for different pavement materials with their standard deviations.

The tricolour ICBP was measured in multiple locations. At Site A and Site B, the albedo remained stable around 0.21. Furthermore, there was a clear reduction in reflectance at Site C, where the albedo of aged ICBP fell to 0.11. This result shows that the cooling effect of reflective pavements is not permanent and can be reduced by ageing and surface dirt. Therefore, maintaining high albedo levels over time requires regular cleaning and maintenance, in addition to careful material selection at the design stage. Without these actions, the expected benefits for UHI mitigation may be significantly reduced in real urban conditions.

The yellow ICBP at Site C showed significant spatial variability. A dirty area measured 0.15, while a cleaner section recorded 0.20. The wavy grey ICBP demonstrated relatively constant performance, with average albedo values of 0.245: in this case, it must be considered that the reflection is reduced by the presence of cracks (13%). The lowest albedo values were recorded for asphalt surfaces, ranging from 0.08 to 0.12.

4.4. Comparison with Satellite Image Sentinel-2 and Landsat 8/9

4.4.1. Satellite Image Selection

This study utilised clear-sky images with cloud cover below 10% from Sentinel-2 and Landsat 8 and 9 to compare conditions before the retrofit of parking pavements in the summer of 2023 and after the retrofit in the summer of 2025. Sentinel-2 images were used to extract high-resolution optical characteristics, including albedo and SRI, while Landsat 8 and 9 images were primarily used to retrieve LST and calculate SUHII.

Acquisition dates were selected to ensure comparable meteorological conditions, as detailed in Tables 3 and 4. Meteorological data were obtained from the Politecnico di Torino weather station at 15 min intervals and aggregated to daily statistics. On these days, the daily mean air temperatures across selected dates ranged from 27.7 °C to 29.5 °C, with daily global solar irradiance between approximately 5800 and 7400 W/m^2.

Table 3. Landsat 8 and 9 acquisitions and meteorological conditions.

Landsat-8/9 Date	Renovation Phase	Mean Air Temperature (°C)	Max Air Temperature (°C)	Min Air Temperature (°C)	Daily Average Solar Irradiance (W·m^{-2})	Landsat 8/9 Image ID
20 August 2023	Before retrofit	28.6	34.8	23.7	5880	LC08_195029_20230820
21 August 2023	Before retrofit	29.5	34.5	25.3	6067	LC09_194029_20230821
1 July 2025	After retrofit	27.7	33.7	22.2	7395	LC08_194029_20250701
1 August 2025	After retrofit	29.4	35.9	23.4	6093	LC09_194029_20250810

Table 4. Sentinel-2 acquisitions matched with Landsat 8/9 and meteorological conditions.

Landsat 8 and 9 Dates	Matched Sentinel 2 Date	Mean Air Temperature (°C)	Max Air Temperature (°C)	Min Air Temperature (°C)	Daily Global Solar Radiation (W·m^{-2})	Sentinel-2 Image ID
20 August 2023	21 August 2023	29.7	35.2	24.8	6024	20230822T102609_20230822T103048_T32TLQ
21 August 2023	10 August 2023	28.7	33.9	23.6	7301	20230710T101609_20230710T102211_T32TLQ
1 July 2025	19 June 2025	27.0	32.6	21.3	7570	20250619T101559_20250619T102452_T32TLQ
1 August 2025	16 August 2025	29.0	35.5	23.4	6180	20250816T103041_20250816T103314_T32TLQ

4.4.2. Albedo Calculation

It is notable that Sentinel-2 bands cover only specific portions of the solar spectrum, whereas ground-based albedo integrates across the entire shortwave range. The spectral response of materials can vary significantly across wavelengths, so some measurement results can also vary.

In addition, as previously discussed in the method, these values reflect the aggregate performance of the parking surface environment, where the presence of vehicles is. Especially, light-coloured cars, like white, could improve the solar reflection [27]. This explains the observed difference between the Sentinel-2 calculated albedo (0.34–0.52) and the in situ measurements (0.11–0.21). Also, for asphalt, its albedo cannot be 0.08; it must be much higher.

Despite these variations, the satellite data clearly validate the impact of the ICBP. As shown in Figure 12 and Table 5, the mean albedo in 2025 was noticeably higher than in 2023 across all sites. Specifically, the mean albedo of Site A, Site B, and Site C increased from 0.36, 0.38, and 0.40 in 2023 to 0.51, 0.51, and 0.49 in 2025.

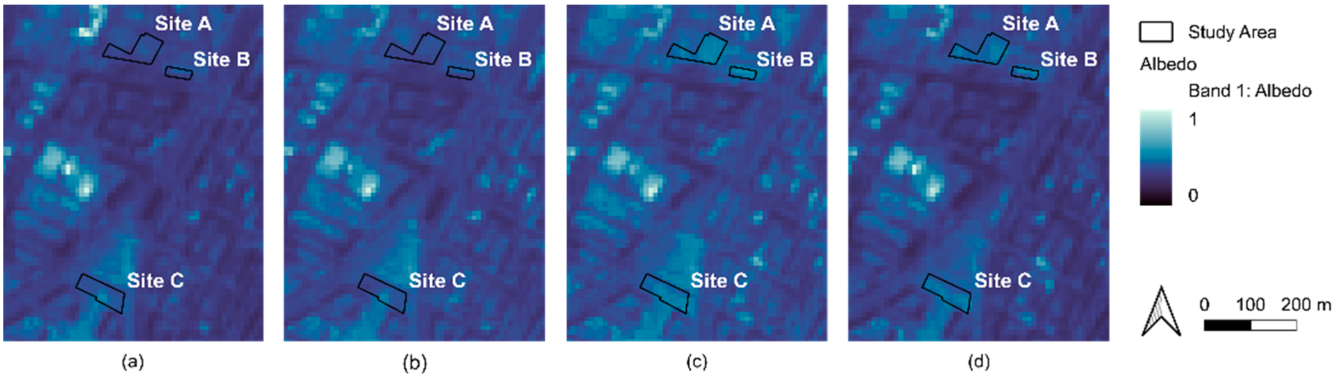

Figure 12. Albedo (–) with resolution 10 m (at ∼10 a.m.) for the days of: (**a**) 20 August 2023; (**b**) 21 August 2023; (**c**) 1 July 2025; and (**d**) 10 August 2025.

Table 5. Albedo statistics by year and location.

Year	Location	Albedo (Date 1)	Albedo (Date 2)	Mean Albedo
2023	Site A	0.39	0.34	0.36
2023	Site B	0.40	0.36	0.38
2023	Site C	0.42	0.38	0.40
2025	Site A	0.50	0.52	0.51
2025	Site B	0.52	0.49	0.51
2025	Site C	0.48	0.49	0.49

4.4.3. SRI Calculation

Remote sensing evaluations derived from Sentinel-2 imagery demonstrate that SRI values in 2025 were significantly higher across all sites compared to 2023, as illustrated in Figure 13. Specifically, Table 6 shows that the average SRIs for Site A, Site B, and Site C in 2023 were 41.93, 43.51, and 46.57, respectively. These values rose to 60.90, 60.68, and 58.36 in 2025. The trend in SRI improvement closely aligns with the observed albedo increase, further validating the effectiveness of higher albedo ICBP materials in improving surface solar reflectance.

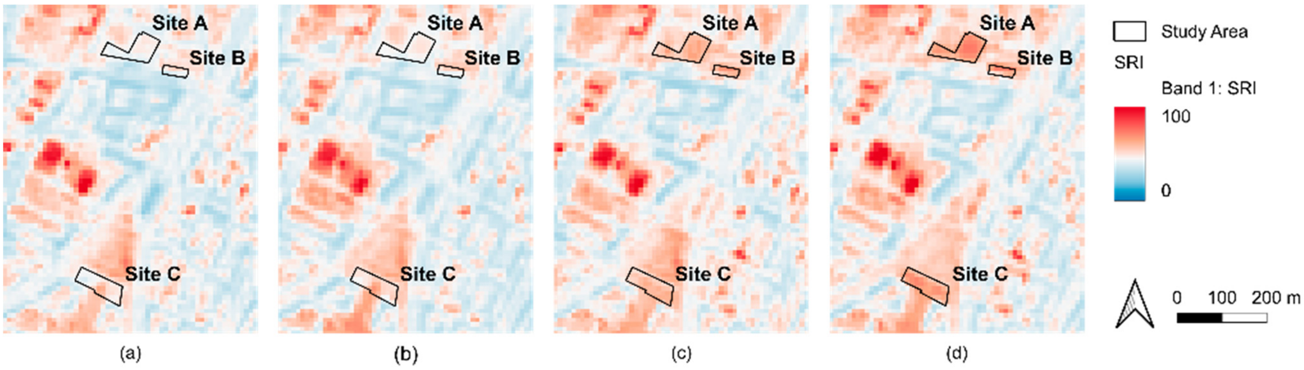

Figure 13. SRI (%) with resolution 10 m (at ∼10 a.m.) for the days of: (**a**) 20 August 2023; (**b**) 21 August 2023; (**c**) 1 July 2025; and (**d**) 10 August 2025.

Table 6. SRI statistics by year and location.

Year	Location	SRI (Date 1), %	SRI (Date 2), %	Mean SRI, %
2023	Site A	45.09	38.78	41.93
2023	Site B	46.32	40.69	43.51
2023	Site C	48.84	44.30	46.57
2025	Site A	59.64	62.15	60.90
2025	Site B	62.47	58.89	60.68
2025	Site C	57.87	58.85	58.36

4.4.4. LST Downscaling and SUHII Calculation

Table 7 summarises the independent validation results of the downscaling model for four dates. Overall, the model demonstrates robust predictive performance, with the coefficient of determination (R^2) consistently being around 0.86, indicating that the selected predictors effectively explain the main spatial variability in land surface temperature across the study area. In terms of error metrics, the RMSE ranges from 2.00 to 2.64, while the MAE remains below 1.20 for all dates. The consistency of accuracy metrics across different years confirms the stability and transferability of the proposed downscaling approach for high-resolution urban thermal environment mapping.

Table 7. Accuracy assessment of the downscaled LST (10 m) across different dates.

Date	R^2	RMSE	MAE
20 August 2023	0.846	2.645	0.993
21 August 2023	0.864	2.409	1.077
1 July 2025	0.863	2.410	1.116
10 August 2025	0.862	2.008	0.956

The validation across different urban uniform areas reveals the precision of the downscaling model. The industrial zones consistently exhibit the highest correlation, as shown in Figure 14, with R^2 values reaching near-perfect levels (0.999 to 1.000). This suggests that the model is particularly effective at capturing the thermal characteristics of large-scale, uniform impervious surfaces. Similarly, high performance is observed in the square ($R^2 \geq 0.991$) and hill ($R^2 \geq 0.992$) categories. In contrast, the model shows slightly lower, yet still robust, performance in the building and river categories. The building category likely reflects the complex thermal environment created by building geometries. The river category highlighted the inherent difficulty in downscaling water bodies, due to the influence of mixed boundary pixels. Despite these minor variations, the consistency of R^2 across all dates and categories confirms the model's strong transferability and spatial stability.

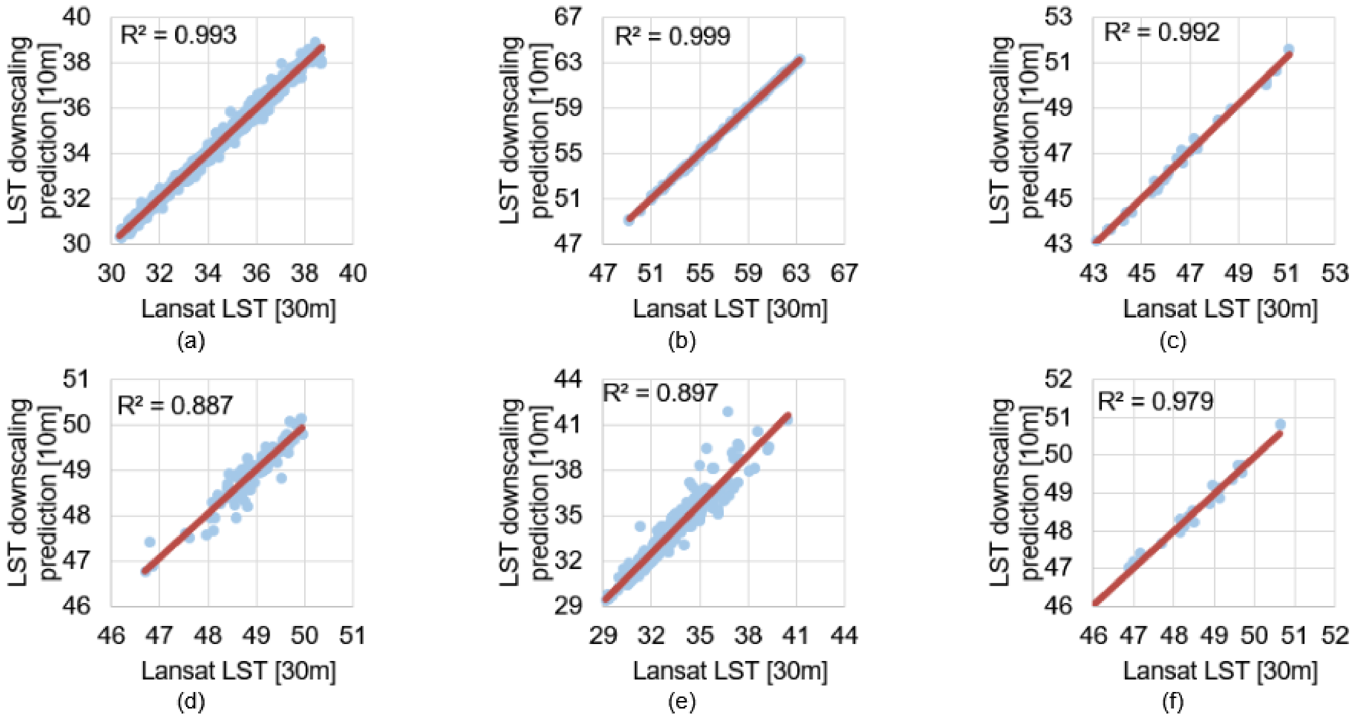

Figure 14. R^2 performance of downscaling modelling of LST (°C) in uniform areas: (**a**) hill; (**b**) industry; (**c**) park; (**d**) building; (**e**) river; and (**f**) square.

Figure 15 provides a visual comparison of the LST products at different scales, focusing on Piazza Vittorio Veneto. While the original 30 m Landsat LST (Figure 15b) only provides a generalised thermal distribution, the 10 m downscaled map (Figure 15c) significantly enhances detail. Specifically, the downscaled version successfully captures the thermal variety within the built-up area, bridge, river and square that were previously blurred at rough resolutions. This improved spatial granularity aligns well with the features that are visible in the high-resolution orthophoto imagery (Figure 15a), demonstrating the model's ability to improve the accuracy of the urban thermal distribution.

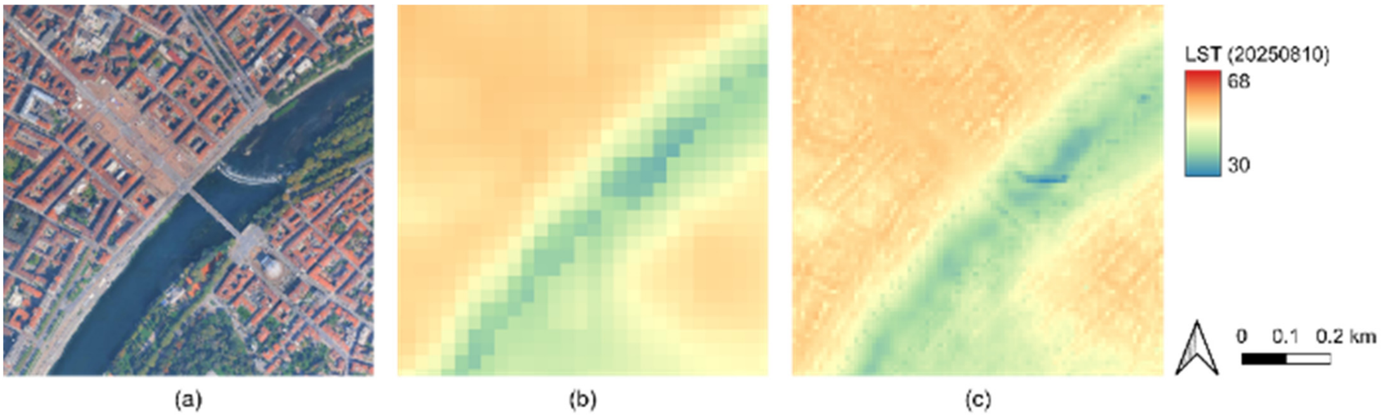

Figure 15. Downscaling of Piazza Vittorio Veneto from the 30 m LST to 10 m resolution on 10 August 2025, at ∼10 a.m.: (**a**) orthophoto image; (**b**) LST (°C) with resolution of 30 m; and (**c**) LST (°C) with resolution of 10 m.

Before focusing on the specific parking areas, the broader thermal context of the city of Turin was analysed. Figures A1 and A2 in Appendix A illustrate the spatial distribution of LST and SUHII on the hottest recorded day (10 August 2025), serving as a reference for the background thermal environment.

In terms of SUHII, values in 2025 were lower than in 2023, indicating a general reduction in surface temperature differences after the retrofit. Figure 16 presents the spatial distribution of SUHII for each period. In the 2025 imagery, the areas of high thermal intensity, especially within Site C, became significantly less intense. This provides further evidence that the UHI effect was partially mitigated following the application of high-albedo materials. Quantitatively, as shown in Table 8, the mean SUHIIs for the three sites in 2023 were 0.95, 0.81, and 0.42, which decreased to 0.87, 0.77, and 0.29 in 2025, respectively.

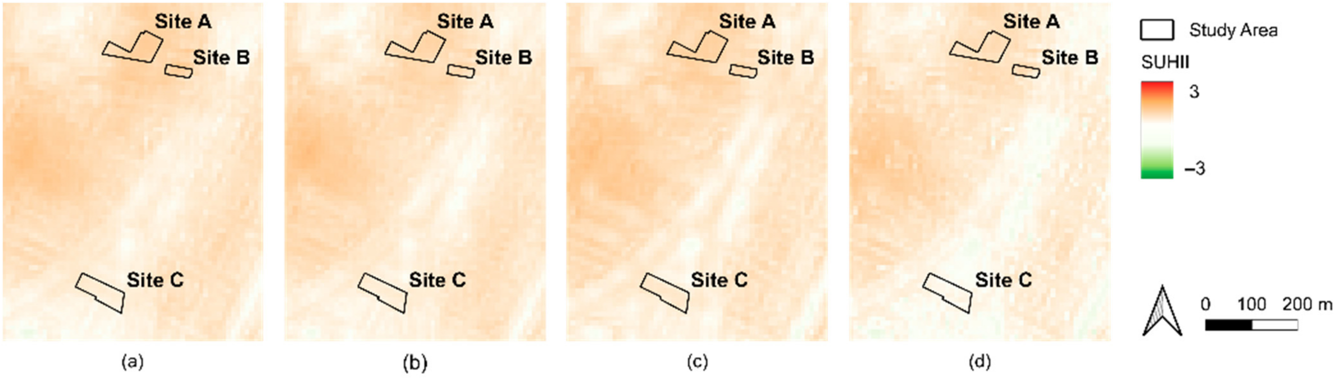

Figure 16. SUHII (–) with resolution 10 m (at ∼10 a.m.) for the days of: (**a**) 20 August 2023; (**b**) 21 August 2023; (**c**) 1 July 2025; and (**d**) 10 August 2025.

Table 8. SUHII statistics by year and location.

Year	Location	SUHII (Date 1)	SUHII (Date 2)	Mean SUHII
2023	Site A	1.08	0.95	0.95
2023	Site B	1.06	0.81	0.81
2023	Site C	0.42	0.42	0.42
2025	Site A	1.07	0.79	0.87
2025	Site B	0.87	0.74	0.77
2025	Site C	0.52	0.16	0.29

https://doi.org/10.3390/su18041876

To further verify the observed trends, the satellite-based results were compared with the findings reported in existing studies. The analysis shows that, relative to the pre-renovation condition in 2023, the renovated parking areas experienced a clear improvement in thermal performance, with an average LST reduction ranging from 4.42 °C to 5.18 °C. This deduction is consistent with the local field study conducted by Rossi et al. (2018) in Turin [36], which reported a maximum surface temperature reduction of approximately 9.0 °C under the local climatic conditions using cool coatings. Although liquid coatings are generally considered to have higher reflective potential than interlocking concrete block pavement, the ICBP applied in this study still achieved a good cooling effect that was comparable to that of reflective coatings.

In contrast, when compared with the benchmarks that were reported globally, the observed cooling potential appears to be relatively moderate. For instance, Kousis and Pisello (2023) [37] reported that reflective pavement technologies can reduce surface temperatures by 3 °C to 20 °C in large-scale applications. The difference between these global values and the result of this study is not solely due to climate thermal variance, but is also due to practical constraints and surface obstructions, including the presence of parked vehicles. A discussion of how these factors influence the analysis accuracy is provided in Section 4.5.

4.5. Field of Application and Future Developments

The measurements campaign of the albedo in car parking areas was developed in four steps: one in a laboratory under test conditions, two on the rooftop of DENERG in a controlled environment, three in situ with free uncovered surfaces of parking areas, and four with satellite images to describe the real use conditions of parking areas.

The measurements of the albedo in the laboratory and on the rooftop of DENERG were guided by ASTM standards and the results also showed good accuracy with the test sample of 1 m^2. In situ, more variables influenced the measurements of the albedo in real parking areas, such as the age of pavements and the presence of shadows, smog and dirt; these results are then site-specific, but they are important to be able to describe the trend of albedo values that decrease in urban environments. Then, with remote-sensing analysis, the real use of pavement material is tested, considering real areas with the presence of cars. Finally, the overall methodology of this analysis can be used to evaluate the characteristics of ICBPs in test and real conditions, but also to monitor their actual and future effects on the urban heat island phenomenon with satellite images.

On the use of remote sensing analysis, some more comments can be added:

- The selection of satellite images is fundamental to controlling errors, especially considering the climate conditions. Output stability depends on cloud cover over both the study area and surrounding regions, as nearby clouds can bias satellite-derived solar reflectance and temperature, relative to fully clear sky conditions.
- Since Sentinel-2 lacks thermal bands, high-resolution LST is derived through downscaling with Landsat data. Differences in acquisition time and climatic conditions may cause inconsistencies in surface states, such as after rainfall, thereby reducing the accuracy of the optical and thermal variables calculation.
- There is a pixel mixing effect that introduces errors into optical and thermal calculations. For instance, white vehicles tend to increase the albedo and SRI values, lowering the observed LST, whereas black vehicles can significantly raise the LST. The presence of vehicles constitutes a limitation when assessing the urban thermal environment using satellite images, as it is impossible to observe the pavement surface material itself in reality.
- The derivation of broadband albedo from Sentinel-2 multi-spectral bands introduces inherent methodological uncertainty. Following the empirical relationship established

by Liang (2001) [38], the conversion from top-of-atmosphere reflectance to broadband surface albedo typically carries an uncertainty of approximately ±0.01 to 0.05.

Future developments of this work will test the ageing effects on ICBPs, according to the ASTM D7897E. Another improvement on actual future scenarios will also consider the reduction in energy consumption and greenhouse gas emissions in the SUHII model [39].

5. Conclusions

This study evaluated the reflective performance of ICBPs in Turin and quantified their potential to mitigate the UHI effects compared to asphalt surfaces. By integrating experimental campaigns, in situ measurements, and satellite remote sensing, the research confirmed that retrofitting parking surfaces significantly enhances their thermal performance. Specifically, during the experimental campaign, the ICBP increased to a mean albedo of ∼0.22, whereas in situ, the ICBP measured a mean albedo of ∼0.20, compared with asphalt at 0.08–0.12, resulting in an average measurable reduction of 15% in SUHII across the study sites, as observed in satellite images. These findings validate the efficacy of cool pavements as a practical strategy for urban climate adaptation.

Overall, the proposed method is built upon a standardised analytical framework and does not depend on city-specific or climate-specific empirical parameters. As a result, it demonstrates a high degree of transferability. The workflow can be applied to areas under different climatic conditions to investigate LST differences induced by pavement materials with varying albedo.

At the same time, the findings indicate that the reliable application of this method depends on specific prerequisites, including relatively stable weather conditions at the regional scale and an appropriate temporal alignment among multiple source satellite images. In climate zones characterised by frequent cloud cover or rainfall, image scenes with predominantly clear conditions should be prioritised, and the temporal gap between different satellite datasets should be minimised to reduce the influence of environmental variability. When these conditions are satisfied, the method can serve as a reproducible and quantitative tool to support the assessment of pavement cooling potential and the development of urban thermal environment mitigation strategies across different cities.

Future research should extend monitoring to support long-term, multi-season, multi-year monitoring, especially by satellite images. This approach would enable the quantification of ageing indicators, such as the rate of albedo decay. Importantly, the monitoring scope should be extended to winter performance to examine thermal performance and thermal comfort, including surface overcooling. In addition, applying this method across different urban contexts, such as residential areas and public squares, would improve the dataset's representativeness. Overall, this framework can provide policymakers with a scientific basis for including high-albedo materials in sustainable urban renewal guidelines to address the rising urban temperatures.

Author Contributions: Conceptualization, G.M.; methodology, X.Z., C.F., G.M.; software, X.Z.; validation, X.Z.; formal analysis, X.Z., C.F., E.C., M.B., G.M.; resources, E.C., M.B., G.M.; writing—original draft preparation, X.Z., C.F., L.T., G.M.; writing—review and editing, X.Z., C.F., L.T., E.C., G.M.; supervision, G.M. All authors have read and agreed to the published version of the manuscript.

Funding: This research received no external funding.

Data Availability Statement: The data supporting the work of this article will be made available by the authors on request.

Conflicts of Interest: The authors declare no conflict of interest.

Abbreviations

The following abbreviations are used in this manuscript:

ASTM	American Society for Testing and Materials
ATPRK	Area-to-Point Regression Kriging
GEE	Google Earth Engine
ICBP	Interlocking Concrete Block Pavement
LEED	Leadership in Energy and Environmental Design
LST	Land Surface Temperature
MAE	Mean Absolute Error
NDBI	Normalised Difference Built-up Index
NDVI	Normalised Difference Vegetation Index
NDWI	Normalised Difference Water Index
NIR	Near-Infrared Spectral Range
R^2	Coefficient of Determination
RMSE	Root Mean Square Error
sol	Solar Spectral Range
SRI	Solar Reflectance Index
SUHI	Surface Urban Heat Island
SUHII	Surface Urban Heat Island Intensity
SWIR	Short Wave Infrared Spectral Range
UHI	Urban Heat Island
uv	Ultraviolet Spectral Range
vis	Visible Spectral Range

Appendix A

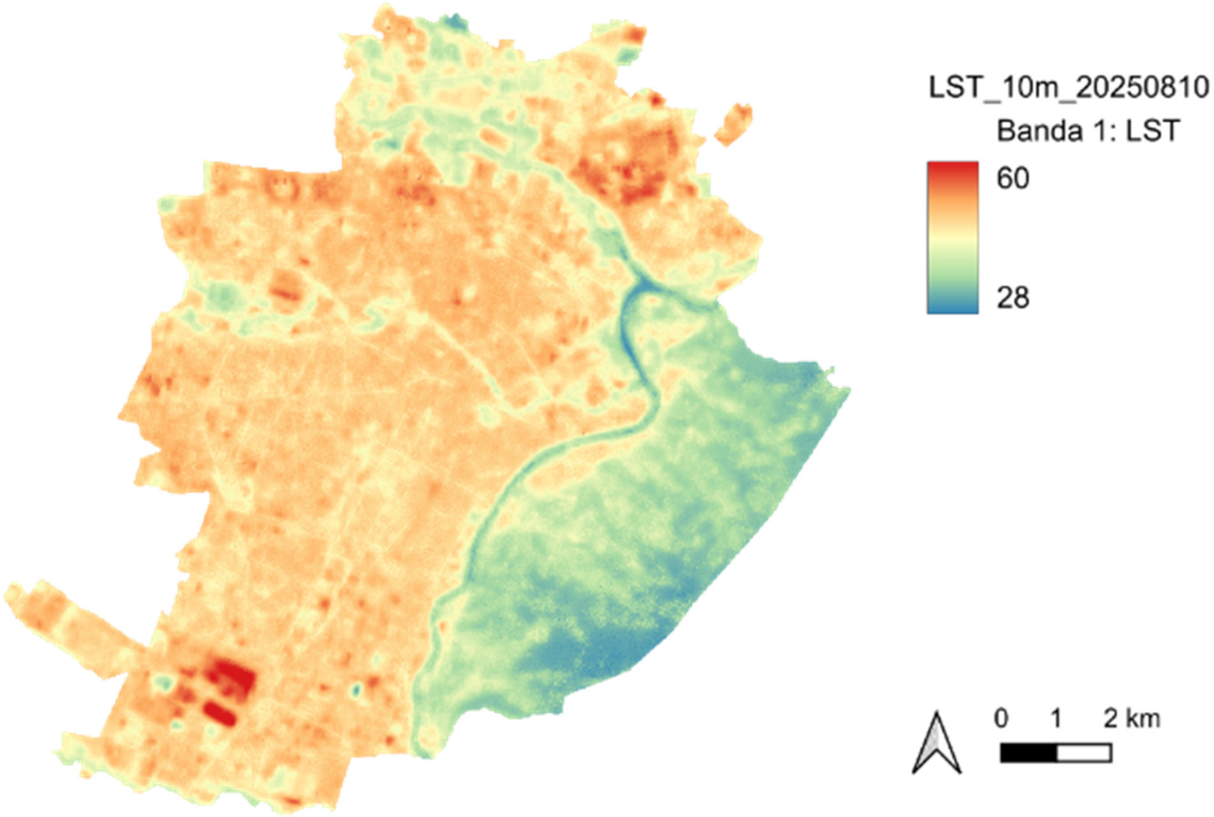

Figure A1. The LST (°C) of Turin at a resolution of 10 m on 10 August 2025.

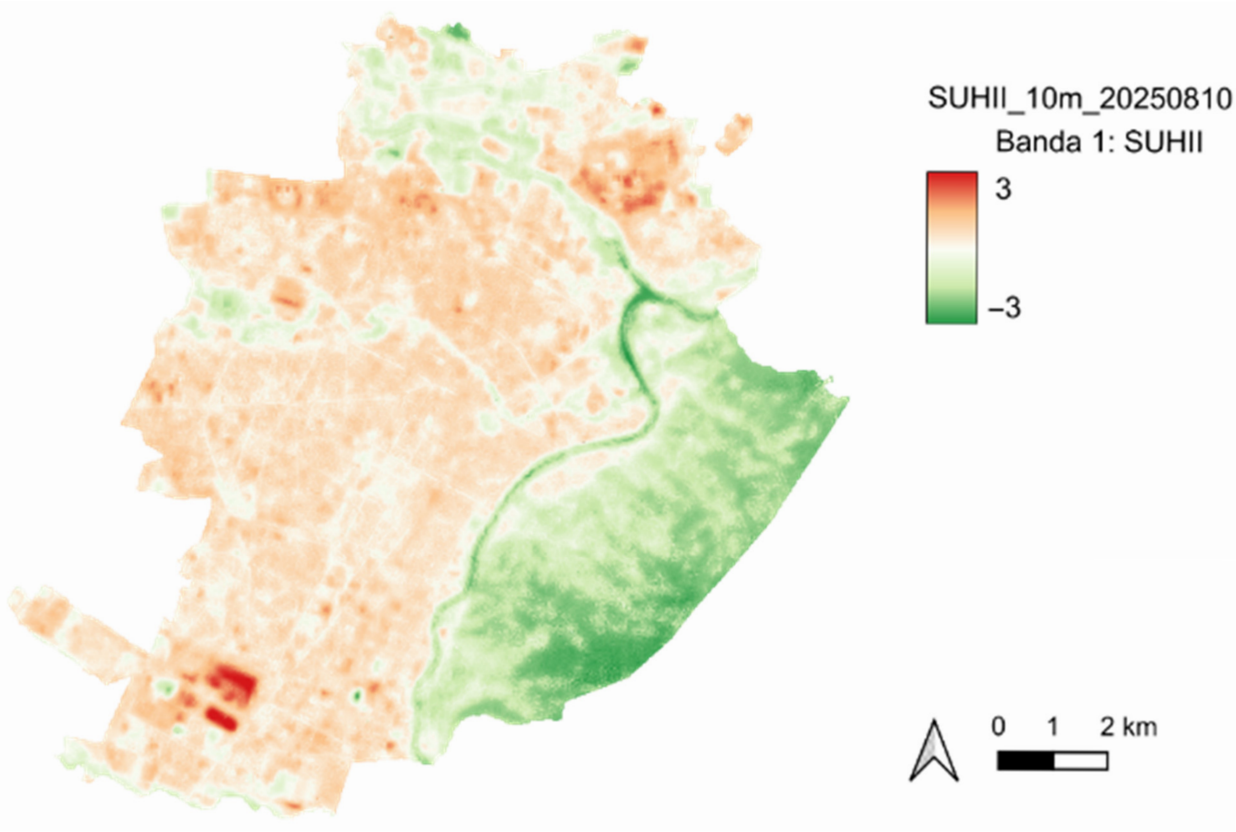

Figure A2. The SUHII (–) of Turin at a resolution of 10 m on 10 August 2025.

References

1. Saikia, P.; Langshiang, D.S.; Raliang, L. Land use and land cover changes and their effect on forest cover dynamics: A CA-ANN model in East Khasi Hills, Meghalaya, India. *J. Environ. Sci. Health Sustain.* **2025**, *1*, 51–64. [CrossRef]
2. Mora, C.; Dousset, B.; Caldwell, I.; Redman, F.; Padmanabhan, C.; Sukalac, M.; Keellings, N.; Shah, H. Global risk of deadly heat. *Nat. Clim. Change* **2017**, *7*, 501–506. [CrossRef]
3. Santamouris, M. Using cool pavements as a mitigation strategy to fight urban heat island—A review of the actual developments. *Renew. Sustain. Energy Rev.* **2013**, *26*, 224–240. [CrossRef]
4. Akbari, H.; Matthews, H.D. Global Cooling Updates: Reflective Roofs and Pavements. *Energy Build.* **2012**, *55*, 598–601. [CrossRef]
5. Nath, B.; Ni-Meister, W.; Özdoğan, M. Fine-scale urban heat patterns in New York City measured by ASTER satellite—The role of complex spatial structures. *Remote Sens.* **2021**, *13*, 3797. [CrossRef]
6. Delmastro, C.; Mutani, G.; Schranz, L.; Vicentini, G. The role of urban form and socio-economic variables for estimating the building energy savings potential at the urban scale. *Int. J. Heat Technol.* **2015**, *33*, 91–100. [CrossRef]
7. *ASTM E1918–21*; Standard Test Method for Measuring Solar Reflectance of Horizontal and Low-Sloped Surfaces in the Field. ASTM International: West Conshohocken, PA, USA, 2021.
8. Qin, Y.; He, H. A New Simplified Method for Measuring the albedo of Limited Extent Targets. *Solar Energy* **2017**, *157*, 1047–1055. [CrossRef]
9. Sen, S.; Roesler, J.; King, D. albedo Estimation of Finite-Sized Concrete Specimens. *J. Test. Eval.* **2019**, *47*, 738–757. [CrossRef]
10. Chen, J.; Zhou, Z.; Wu, J.; Hou, S.; Liu, M. Field and Laboratory Measurement of albedo and Heat Transfer for Pavement Materials. *Constr. Build. Mater.* **2019**, *202*, 46–57. [CrossRef]
11. Mainieri, J.J.G.; Sen, S.; Roesler, J.R.; Al-Qadi, I.L. albedo Change Mechanism of Asphalt Concrete Surfaces. *Transp. Res. Rec. J. Transp. Res. Board* **2022**, *2676*, 763–772. [CrossRef]
12. Santamouris, M.; Gaitani, N.; Spanou, A.; Saliari, M.; Giannopoulou, K.; Vasilakopoulou, K.; Kardomateas, T. Using cool paving materials to improve microclimate of urban areas—Design realization and results of the flisvos project. *Build. Environ.* **2012**, *53*, 128–136. [CrossRef]
13. Sen, S.; Roesler, J.; Ruddell, B.; Middel, A. Cool Pavement Strategies for Urban Heat Island Mitigation in Suburban Phoenix, Arizona. *Sustainability* **2019**, *11*, 4452. [CrossRef]
14. Schneider, F.A.; Ortiz, J.C.; Vanos, J.K.; Sailor, D.J.; Middel, A. Evidence-based guidance on reflective pavement for urban heat mitigation in Arizona. *Nat. Commun.* **2023**, *14*, 1467. [CrossRef]

15. Elmagri, H.; Kamel, T.M.; Ozer, H. Assessment of the effectiveness of cool pavements on outdoor thermal environment in urban areas. *Build. Environ.* **2024**, *266*, 112095. [CrossRef]
16. Andrés-Anaya, P.; Sánchez-Aparicio, M.; del Pozo, S.; Lagüela, S. Correlation of land surface temperature with IR albedo for the analysis of urban heat island. *Eng. Proc.* **2021**, *8*, 9. [CrossRef]
17. Despini, F.; Ferrari, C.; Santunione, G.; Tommasone, S.; Muscio, A.; Teggi, S. Urban surfaces analysis with remote sensing data for the evaluation of UHI mitigation scenarios. *Urban Clim.* **2021**, *35*, 100761. [CrossRef]
18. Muscio, A. The Solar Reflectance Index as a Tool to Forecast the Heat Released to the Urban Environment: Potentiality and Assessment Issues. *Climate* **2018**, *6*, 12. [CrossRef]
19. *E1980-24*; Standard Practice for Calculating Solar Reflectance Index of Horizontal and Low-Sloped Opaque Surfaces. ASTM International: West Conshohocken, PA, USA, 2024.
20. *C1549-16*; Standard Test Method for Determination of Solar Reflectance Near Ambient Temperature Using a Portable Solar Reflectometer. ASTM International: West Conshohocken, PA, USA, 2022.
21. *E903-20*; Standard Test Method for Solar Absorptance, Reflectance, and Transmittance of Materials Using Integrating Spheres. ASTM International: West Conshohocken, PA, USA, 2020.
22. Ferrari, C.; Libbra, A.; Muscio, A.; Siligardi, C. Influence of the irradiance spectrum on solar reflectance measurements. *Int. J. Smart Nano Mater.* **2013**, *4*, 244–253. [CrossRef]
23. Synnefa, A.; Pantazaras, A.; Santamouris, M.; Bozonnet, E.M.D.; Doya, M.; Zinzi, M.; Muscio, A.; Libbra, A.; Ferrari, C.; Coccia, V.; et al. Interlaboratory Comparison of Cool Roofing Material Measurement Methods. In Proceedings of the 34th AIVC Conference, Athens, Greece, 25–26 September 2013.
24. *ISO 9847:2023*; Solar energy—Calibration of Pyranometers by Comparison to a Reference Pyranometer. International Organization for Standardization: Geneva, Switzerland, 2023.
25. Levinson, R.; Akbari, H.; Berdahl, P. Measuring Solar Reflectance—Part II: Review of Practical Methods. *Sol. Energy* **2010**, *84*, 1964–1979. [CrossRef]
26. Akbari, H.; Levinson, R.; Stern, S. Procedure for Measuring the Solar Reflectance of Flat or Curved Roofing Assemblies. *Sol. Energy* **2008**, *82*, 648–660. [CrossRef]
27. Matias, M.; Mills, G.; Silva, T.; Girotti, C.; Lopes, A. The underestimated impact of parked cars in urban warming. *City Environ. Interact.* **2025**, *26*, 100232. [CrossRef]
28. Mutani, G.; Scalise, A.; Sufa, X.; Grasso, S. Synergising Machine Learning and Remote Sensing for Urban Heat Island Dynamics: A Comprehensive Modelling Approach. *Atmosphere* **2024**, *15*, 1435. [CrossRef]
29. Wang, Q.; Shi, W.; Atkinson, P.M. Area-to-point regression kriging for pan-sharpening. *ISPRS J. Photogramm. Remote Sens.* **2016**, *114*, 151–165. [CrossRef]
30. ARPA Piemonte. *Dati Meteorologici Storici e Climatologici Della Regione Piemonte*; Agenzia Regionale per la Protezione Ambientale del Piemonte: Torino, Italy. Available online: https://www.arpa.piemonte.it (accessed on 5 February 2026).
31. Città di Torino. *Piano di Resilienza Climatica della Città di Torino*; Città di Torino: Torino, Italy, 2020. Available online: https://www.torinovivibile.it/wp-content/uploads/2021/06/PianoResilienzaClimatica_TORINO.pdf (accessed on 5 February 2026).
32. Mutani, G.; Todeschi, V.; Beltramino, S. Improving Outdoor Thermal Comfort in Built Environment: Assessing the Impact of Urban Form and Vegetation. *Int. J. Heat Technol.* **2022**, *40*, 23–31. [CrossRef]
33. Muttaqii, M.A.; Amin, M.; Handoko, A.S.; Birawidha, D.C.; Isnugroho, K.; Hendronursito, Y.; Niken, R.; Syafriadi. The characterization and physical properties of paving block products over basalt minerals. *AIP Conf. Proc.* **2020**, *2232*, 050006. [CrossRef]
34. Tefa, L.; Coppola, B.; Palmero, P.; Bassani, M. Mechanical properties, life-cycle assessment, and costs of alternative sustainable binders to stabilise recycled aggregates. *Clean. Mater.* **2025**, *15*, 100302. [CrossRef]
35. Camera di Commercio di Torino. Prezzario Opere Edili ed Impiantistiche sulla Piazza di Torino. Available online: https://www.to.camcom.it/prezzario-opere-edili (accessed on 5 January 2026).
36. Rossi, G.; Iacomussi, P.; Zinzi, M. Lighting implications of urban mitigation strategies through cool pavements: Energy savings and visual comfort. *Climate* **2018**, *6*, 26. [CrossRef]
37. Kousis, I.; Pisello, A.L. Evaluating the performance of cool pavements for urban heat island mitigation under realistic conditions: A systematic review and meta-analysis. *Urban Clim.* **2023**, *49*, 101470. [CrossRef]
38. Liang, S. Narrowband to broadband conversions of land surface albedo I: Algorithms. *Remote Sens. Environ.* **2001**, *76*, 213–238. [CrossRef]
39. Carlin, A.; Lo Verso, V.R.M.; Invernizzi, S.; Polato, A. Optimised daylighting for comfort and energy saving for the factory of the future. *Int. J. Mech. Control* **2017**, *18*, 15–29.